

Modeling the Stochastic Gating of Ion Channels

Gregory D. Smith

In previous chapters we have seen several kinetic diagrams representing various molecular states and transitions between these states due to conformational changes and the binding or unbinding of ligands. Up to this point we have assumed a large number of molecules and written rate equations consistent with these transition-state diagrams. But how should we interpret a transition-state diagram when we are considering only a single molecule or a small number of molecules? The short answer to this question is that transition rates can be interpreted as transition probabilities per unit time.

11.1 Single-Channel Gating and a Two-State Model

The time course of voltage changes in a whole cell is the result of the average behavior of many individual channels. Our understanding of individual channel gating comes largely from experiments using the patch clamp technique (see Figure 11.1). For example, typical measurements from a so-called on-cell patch of T-type calcium currents in guinea pig cardiac ventricular myocytes are shown in the middle panel of Figure 11.2. The small current deviations in the negative direction indicate the opening of individual T-type calcium channels gating in response to a command membrane voltage stepped from -70 mV to -20 mV (top panel). Notice that two conductance states of the channel are visible: a closed state with no current flowing and an open state with unitary current of $\approx 10^{-12}$ amperes (1 picoampere or 1 pA). While transitions between these two conductance states are random in time, the mean of several hundred records (bottom panel of Figure 11.2) smoothes out these current fluctuations and demonstrates that *on*

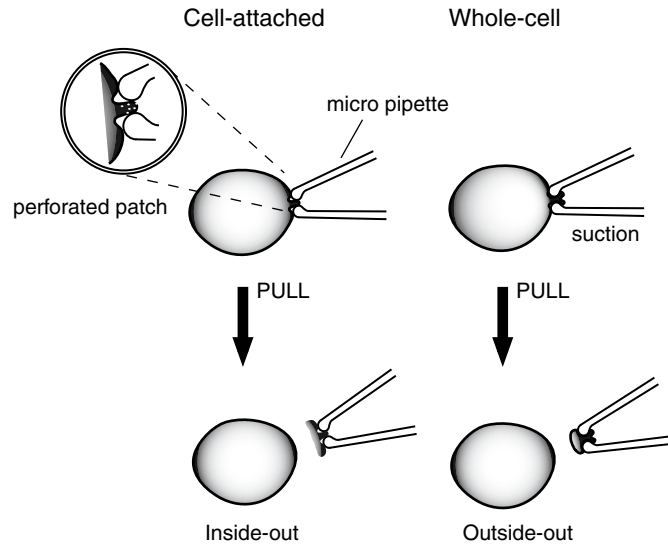
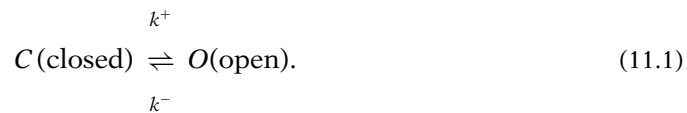


Figure 11.1 Four methods of measuring electrical responses in cells with the patch clamp technique. In the patch technique, a pipette with an opening of $\approx 1 \mu\text{m}$ is used to make a high-resistance (“gigaohm” = 10^9 ohm) seal onto a cellular membrane. In the on-cell patch configuration all the current into the pipette flows directly through the patch, which can contain as few as one or two ion channels. In the whole-cell configuration, the patch is broken and a more accurate whole cell recording can be made as compared with a relatively leaky sharp electrode puncture. In a perforated patch configuration, an ionophore such as nystatin is introduced into the pipette in order to allow whole-cell-like access while minimizing exchange of the cell contents with the contents of the pipette. Alternatively, patches of membrane can be torn off, leading to inside-out and outside-out patches that can be studied in isolation. Adapted from Hille (2001).

average the stochastically gating channel activates and subsequently inactivates with time constants of ≈ 5 ms and 50 ms, respectively. Interestingly, the average dynamics of individual T-type calcium channels is strikingly similar to “whole cell” measurements of the activation and inactivation of T-type calcium currents.

11.1.1 Modeling Channel Gating as a Markov Process

The stochastic gating of a single ion channel can be modeled as a continuous-time Markov process. Consider the simple transition-state diagram encountered first in Chapter 1, the kinetic scheme for ion channel with two states, one closed (C) and the other open (O),



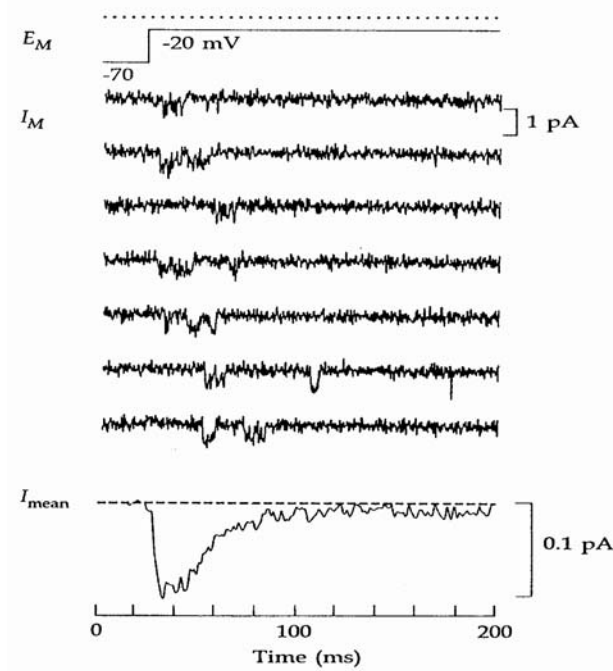


Figure 11.2 On-cell patch clamp measurements of T-type calcium currents in guinea pig cardiac ventricular myocytes. The upper recordings show currents due to one (or a few) stochastically gating single channels when the command voltage is stepped from -70 mV to -20 mV. The lower plot is an average of several hundred such records that shows rapid activation followed by slow inactivation, proportional to macroscopic T-type calcium currents measured in whole-cell configuration. Reprinted from Hille (2001).

Define s to be a random variable taking values $s \in \{C, O\}$ corresponding to these two states, and write $\text{Prob}\{s = i, t\}$ (or for short, $P_i(t)$) to represent the probability that $s(t) = i$; that is, the molecule is in state i at time t . Because the molecule must always be in one of the two states, total probability must be conserved and we have

$$P_C(t) + P_O(t) = 1.$$

Now consider the possibility that the two-state ion channel is in state C at time t . If this is the case, then the rate k^+ (e.g., with units of ms^{-1}) is related to the probability that in a short interval of time (Δt) the two-state ion channel will open. The relationship is given by

$$k^+ \Delta t = \text{Prob}\{s = O, t + \Delta t | s = C, t\}, \quad (11.2)$$

where $k^+ \Delta t$ is dimensionless (a pure number) and $\text{Prob}\{s = O, t + \Delta t | s = C, t\}$ is a shorthand notation for the probability, given that the channel is closed at time t , of a $C \rightarrow O$ transition occurring in the interval $[t, t + \Delta t]$. Multiplying by $P_C(t)$, the probability that the ion channel is indeed in state C , we find that $k^+ P_C(t) \Delta t$ is the probability that the transition $C \rightarrow O$ actually occurs.

The transition-state diagram (11.1) indicates two possible ways for the ion channel to enter or leave the closed state. Accounting for both of these, we have

$$P_C(t + \Delta t) = P_C(t) - k^+ P_C(t) \Delta t + k^- P_O(t) \Delta t.$$

Writing a similar equation relating $P_O(t + \Delta t)$ and $P_O(t)$ and taking the limit $\Delta t \rightarrow 0$ gives the system of ODEs

$$\frac{dP_C}{dt} = -k^+P_C + k^-P_O, \quad (11.3)$$

$$\frac{dP_O}{dt} = +k^+P_C - k^-P_O. \quad (11.4)$$

Because conservation of probability ensures that $P_C(t) = 1 - P_O(t)$, (11.3) can be eliminated to give

$$\frac{dP_O}{dt} = k^+(1 - P_O) - k^-P_O.$$

Note that the similarity of this equation to (1.4), the kinetic equation derived in Chapter 1, is not accidental. The equation governing changes in probabilities for a single molecule always has the same form as the rate equation for a large number of molecules.

11.1.2 The Transition Probability Matrix

From our analysis of the two-state ion channel above, we know that for a channel closed at time t , $k^+\Delta t$ is the probability that it undergoes a transition and opens in the time interval $[t, t + \Delta t]$, provided that Δt is small. By conservation, we also know that the probability that the channel remains closed during the same interval is $1 - k^+\Delta t$. Because a similar argument applies when the channel is open at time t , we can write the *transition probability matrix*

$$Q = \begin{bmatrix} \text{Prob}\{C, t + \Delta t | C, t\} & \text{Prob}\{C, t + \Delta t | O, t\} \\ \text{Prob}\{O, t + \Delta t | C, t\} & \text{Prob}\{O, t + \Delta t | O, t\} \end{bmatrix} = \begin{bmatrix} 1 - k^+\Delta t & k^-\Delta t \\ k^+\Delta t & 1 - k^-\Delta t \end{bmatrix}, \quad (11.5)$$

where the elements of Q_{ij} (row i , column j) correspond to the transition probability from state j to state i , and conservation of probability ensures that all the columns sum to one, that is, for each column j ,

$$\sum_i Q_{ij} = 1. \quad (11.6)$$

The transition probability matrix is especially useful when we write the current state of the channel as the vector

$$\vec{P}(t) = \begin{bmatrix} \text{Prob}\{C, t\} \\ \text{Prob}\{O, t\} \end{bmatrix}. \quad (11.7)$$

Using this notation, the state of the channel at $t + \Delta t$ is given by the matrix multiplication

$$\vec{P}(t + \Delta t) = Q\vec{P}(t). \quad (11.8)$$

For example, if the channel is known to be closed at time t , then

$$\vec{P}(t) = \begin{bmatrix} 1 \\ 0 \end{bmatrix},$$

and the distribution of probability after one time step is

$$\vec{P}(t + \Delta t) = \begin{bmatrix} 1 - k^+ \Delta t & k^- \Delta t \\ k^+ \Delta t & 1 - k^- \Delta t \end{bmatrix} \begin{bmatrix} 1 \\ 0 \end{bmatrix} = \begin{bmatrix} 1 - k^+ \Delta t \\ k^+ \Delta t \end{bmatrix}.$$

Applying (11.8) iteratively, we see that if the channel is closed at time t , the probability that it is closed or open at time $t + 2\Delta t$ is given by

$$\vec{P}(t + 2\Delta t) = Q [Q\vec{P}(t)], = Q^2\vec{P}(t)$$

or more generally,

$$\vec{P}(t + n\Delta t) = Q^n \vec{P}(t). \quad (11.9)$$

This iterative procedure can be used to calculate the evolution of the probability that the two-state channel is in an open or closed state. It amounts to using Euler's method to integrate (11.3) and (11.4).

11.1.3 Dwell Times

Using the transition probability matrix, it is possible to derive an expression for the average amount of time that the channel remains in the open or closed state, i.e., the open and closed *dwell times*. We have already seen that if a channel is closed at time t , the probability that it remains closed at time $t + \Delta t$ is $1 - k^+ \Delta t$. The probability that the channel remains closed for the following time step as well is thus $(1 - k^+ \Delta t)^2$. In general, we can write

$$\text{Prob}\{C, [t, t + n\Delta t] | C, t\} = (1 - k^+ \Delta t)^n. \quad (11.10)$$

This expression is actually much simpler than (11.9) because here we are insisting that the channel remain closed for the entire interval $[t, t + n\Delta t]$, while (11.9) accounts for the possibility that the channel changes states multiple times. If we define $\tau = n\Delta t$, we can rewrite (11.10) as

$$\text{Prob}\{C, [t, t + \tau] | C, t\} = \left(1 - \frac{k^+ \tau}{n}\right)^n,$$

which is an approximate expression that becomes more accurate (for fixed τ) as $\Delta t \rightarrow 0$ and $n \rightarrow \infty$ simultaneously. Taking this limit and using

$$\lim_{n \rightarrow \infty} \left(1 - \frac{\alpha}{n}\right)^n = e^{-\alpha},$$

we obtain

$$\text{Prob}\{C, [t, t + \tau] | C, t\} = e^{-k^+ \tau}. \quad (11.11)$$

Thus, the probability that a channel closed at time t remains closed until $t + \tau$ is a decreasing exponential function of τ .

In order to complete our calculation of the closed dwell time for the two-state channel, we must consider the probability that a channel closed at time t stays closed during the interval $[t, t + \tau]$ and then opens for the first time in the interval $[t + \tau, t + \tau + \Delta t]$. This probability is given by

$$\text{Prob}\{C, [t, t + \tau] | C, t\} \text{Prob}\{O, t + \tau + \Delta t | C, t + \tau\} = e^{-k^+ \tau} k^+ \Delta t.$$

Thus, the average closed time will be given by

$$\langle \tau_C \rangle = \int_0^\infty \tau e^{-k^+ \tau} k^+ d\tau = \frac{1}{k^+},$$

where we have used

$$\int_0^\infty t e^{-t} dt = 1.$$

Similarly, the average open time of the two-state channel model is

$$\langle \tau_O \rangle = \int_0^\infty \tau e^{-k^- \tau} k^- d\tau = \frac{1}{k^-}.$$

11.1.4 Monte Carlo Simulation

The elements Q_{ij} of the transition probability matrix represent the probability of making a transition from state j to state i in a time step of duration Δt . A simple method for simulating the transitions of a two-state channel is based on (11.6). Because conservation of probability ensures that each column of Q will sum to unity, we can divide the interval $[0, 1]$ into regions, each corresponding to a possible change of state (or lack of change of state). Next, we choose a random number Y uniformly distributed on the interval $[0, 1]$, and make a transition (or not) based upon the subinterval in which Y falls. For example, let us return to the transition probability matrix for the two-state channel given by (11.5). If the current state is O (open), then a transition to the closed state occurs if $0 \leq Y < k^- \Delta t$, while the channel remains open if $k^- \Delta t \leq Y \leq 1$, an interval of length $1 - k^- \Delta t$. Similarly, if the channel is closed, it remains closed if $0 \leq Y < 1 - k^+ \Delta t$, and a transition to the open state occurs if $1 - k^+ \Delta t \leq Y \leq 1$.

Several example simulations of stochastic gating of a two-state channel model using the Monte Carlo method are shown in Figure 11.3. By comparing open probabilities and dwell times in the three simulations shown, one can see how the transition probabilities k^+ and k^- lead to distinct channel kinetics. In Exercise 10 the reader can use the Monte Carlo method to simulate a more complicated model, the four-state GLUT transporter model discussed in Section 3.1.

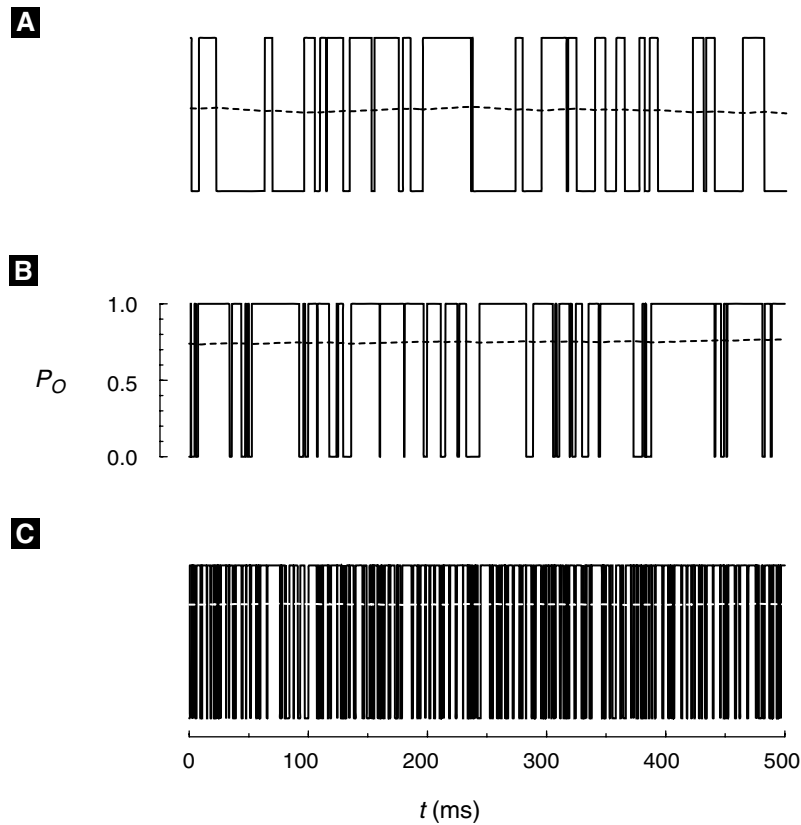


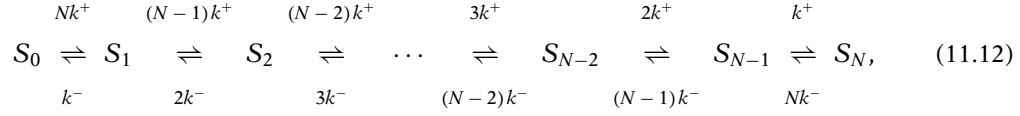
Figure 11.3 A Monte Carlo simulation of the two-state ion channel. (A) $k^+ = 0.1/\text{ms}$, $k^- = 0.1/\text{ms}$, giving an equilibrium open probability (dotted lines) of 0.5. (B) k^+ changed to $0.3/\text{ms}$, and now the equilibrium open probability is 0.75. (C) Transition probabilities increased by factor of 5 ($k^+ = 1.5/\text{ms}$, $k^- = 0.5/\text{ms}$). Note that average open time and average close time are shorter in this case, as evidenced by many more transitions between states.

11.1.5 Simulating Multiple Independent Channels

The gating of multiple independent channels can be simulated in one of several ways. An obvious possible method for simulating a small number of independent two-state ion channels is to implement N Markov variables with identical transition probability matrices given by (11.5).

Under the assumption of identical and independent channels, an alternative method is to simulate a single Markov process that accurately tracks the number of open channels. Note that for an ensemble of N two-state ion channels there are $N + 1$ possibilities for the number of open channels (i.e., $\{0, 1, 2, \dots, N - 2, N - 1, N\}$) and thus $N + 1$ distinguishable states for the ensemble. If we label these states S_0 through S_N ,

we can write the transition-state diagram



where the factors modifying the rate constants k^+ and k^- account for combinatorics. For example, the transition probability Nk^+ leading out of state S_0 accounts for the fact that any one of N closed channels can open (at rate k^+), resulting in one open channel and ensemble configuration S_1 .

The transition probability matrix for the Markov process diagrammed in (11.12) is tridiagonal

$$Q = \begin{bmatrix}
 D_0 & k^- \Delta t & & & & & & & & & \\
 Nk^+ \Delta t & D_1 & & & & & & & & & \\
 & (N-1)k^+ \Delta t & & & & & & & & & \\
 & & \ddots & & & & & & & & \\
 & & & \ddots & & & & & & & \\
 & & & & (N-1)k^- \Delta t & & & & & & \\
 & & & & D_{N-1} & Nk^- \Delta t & & & & & \\
 & & & & k^+ \Delta t & D_N & & & & &
 \end{bmatrix}, \quad (11.13)$$

where the diagonal terms are such that probability is conserved and each column sums to 1:

$$\begin{aligned}
 D_0 &= 1 - Nk^+ \Delta t, \\
 D_1 &= 1 - k^- \Delta t - (N-1)k^+ \Delta t, \\
 D_{N-1} &= 1 - (N-1)k^- \Delta t - k^+ \Delta t, \\
 D_N &= 1 - Nk^- \Delta t.
 \end{aligned}$$

The reader is encouraged to implement a simulation of a small number (e.g., $N = 4$) of identical and independent two-state channels.

11.1.6 Gillespie's Method

Both of the simulation methods described above involve iterating a transition probability matrix and can be quite cumbersome when the number of ion channels being considered is large. Fortunately, an alternative that works well for large N has been devised (Gillespie 1977).

Consider a single two-state ion channel obeying the transition-state diagram (11.1) and recall that the probability that a channel closed at time t remains closed until $t + \tau$ is an exponentially decreasing function of τ given by (11.11). Thus the closed dwell time (τ_C) of the two-state channel is an exponentially distributed random variable; that

is, the probability distribution function of τ_C is

$$\text{Prob}\{\tau < \tau_C \leq \tau + d\tau\} = k^+ e^{-k^+ \tau} d\tau.$$

Similarly, the open dwell time (τ_O) of the channel is an exponentially distributed random variable with probability distribution function

$$\text{Prob}\{\tau < \tau_O \leq \tau + d\tau\} = k^- e^{-k^- \tau} d\tau.$$

Thus, we can simulate a two-state ion channel by alternately choosing open and closed dwell times consistent with these distributions. If one has no subroutine for simulating an exponentially distributed random variable, simply choose a uniformly distributed random variable U on the interval $[0,1]$ and use the relations

$$\begin{aligned}\tau_C &= -\frac{1}{k_+} \ln U, \\ \tau_O &= -\frac{1}{k_-} \ln U.\end{aligned}$$

Gillespie's method is much faster computationally than the Monte Carlo methods described above. Furthermore, because there is no time step involved, the method is exact.

Gillespie's method becomes more involved when the transition-state diagram indicates that more than one possible transition contributes to the dwell time for a given state. This possibility is handled by first choosing an exponentially distributed random number for the dwell time that accounts for all of the possible transitions out of the current state (i.e., using the sum of the transition probabilities). After the length of the dwell time in the current state is thus determined, the destination state is selected by choosing a uniformly distributed random variable on an appropriately partitioned interval, a process similar to the selection of transitions during Monte Carlo simulation (see Section 11.1.4).

11.2 An Ensemble of Two-State Ion Channels

In the previous section we claimed that the equation governing changes in probabilities for a single molecule has the same form as the rate equation for a large number of molecules. This connection can be made more rigorous by specifying the number of molecules we are considering in advance. To simplify calculations we will again consider the two-state ion channel diagrammed in (11.1).

11.2.1 Probability of Finding N Channels in the Open State

Let us write N as the number of molecules, and let $P_O(n, t)$ and $P_C(n, t)$ be the probabilities of having n molecules in states O and C , respectively. Because we will ultimately be

interested in the statistics of current fluctuations, we will focus our attention on $P_O(n, t)$. In any case, the presence of n open channels implies $N - n$ closed channels, i.e.,

$$P_C(n, t) = P_O(N - n, t) \quad (0 \leq n \leq N).$$

Assume that all N molecules are independent and consider a time interval $[t, t + \Delta t]$ short enough that only one molecule has appreciable probability of making a $C \rightarrow O$ or $O \rightarrow C$ transition. During this short time interval, there are four events that can influence $P_O(n, t)$, the probability that there are n open channels. For example, it is possible that there are currently n open channels, and during the time interval $[t, t + \Delta t]$ one of these channels closes. This probability is given by

$$\text{loss}_- = k^- n P_O(n, t) \Delta t,$$

where the parameter k^- is the transition probability for $O \rightarrow C$, $P_O(n, t)$ is the probability that there were n open channels to begin with, and the n scales this probability to account for the fact that any one of the n independent open channels can close with equivalent result. Similar reasoning leads to the expression

$$P_O(n, t + \Delta t) = P_O(n, t) + \text{gain}_+ - \text{loss}_+ + \text{gain}_- - \text{loss}_-, \quad (11.14)$$

where

$$\begin{aligned} \text{gain}_- &= k^-(n+1)P_O(n+1, t)\Delta t, \\ \text{loss}_+ &= k^+(N-n)P_O(n, t)\Delta t, \\ \text{gain}_+ &= k^+(N-n+1)P_O(n-1, t)\Delta t. \end{aligned}$$

To give one more example, the gain_+ term in this equation represents a probability flux due to the possibility that there are $n - 1$ open channels and one of the closed channels opens. This transition probability is given by $k^+(N - n + 1)P_O(n - 1, t)\Delta t$, because any one of the $N - (n - 1) = N - n + 1$ closed channels can open with equivalent result.

Taking the limit $\Delta t \rightarrow 0$ of (11.14) gives the ordinary differential equation

$$\begin{aligned} \frac{d}{dt}P_O(n, t) &= k^+(N - n + 1)P_O(n - 1, t) - k^+(N - n)P_O(n, t) \\ &\quad + k^-(n + 1)P_O(n + 1, t) - k^- n P_O(n, t). \end{aligned} \quad (11.15)$$

This rather complicated expression is called a *master equation*. It actually represents $N + 1$ coupled ordinary differential equations, one for each $P_O(n, t)$ for $0 \leq n \leq N$ (all possible values for the number of open channels).

The equilibrium solution to the master equation is $N + 1$ time-independent probabilities $P_O^\infty(n)$, given by the binomial distribution

$$P_O^\infty(n) = \binom{N}{n} p^n (1 - p)^{N-n}, \quad (11.16)$$

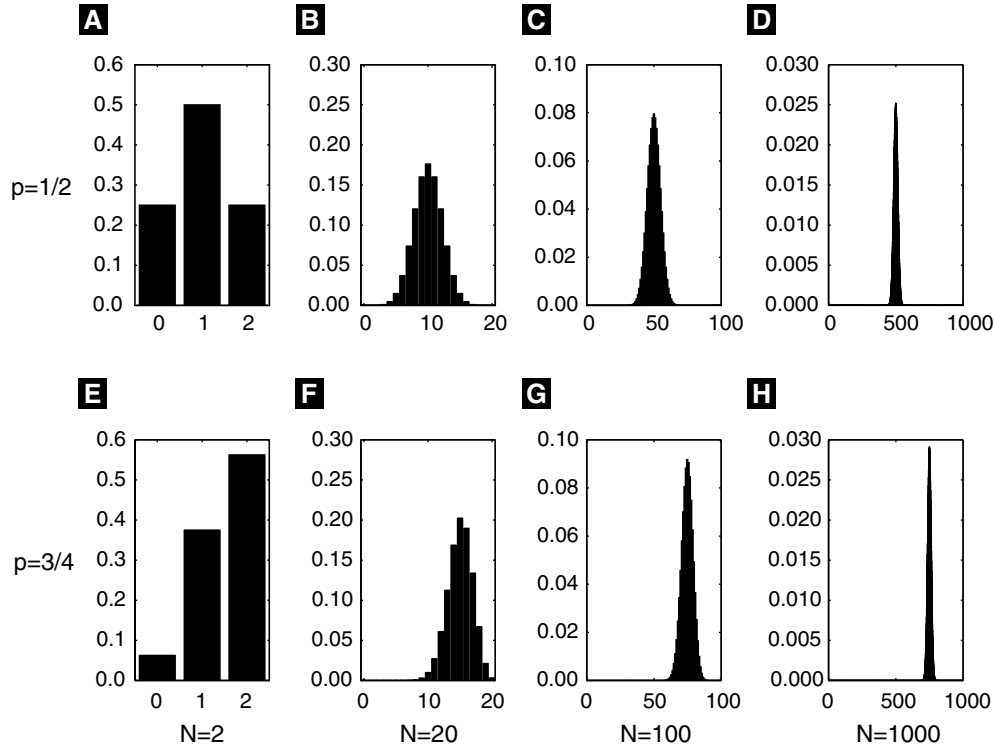


Figure 11.4 For an equilibrium ensemble of N two-state channels with open probability p , the likelihood of observing n open channels is given by the binomial probability distribution (11.16), with parameters N and p . The binomial probability distribution has mean Np , variance $Np(1-p)$, and coefficient of variation $[(1-p)/Np]^{1/2}$. Note that as the equilibrium open probability, p , increases the mean number of open channels shifts rightward. The $N^{-1/2}$ factor in the coefficient of variation is reflected in the narrowing of the distributions (from left to right).

where $p = k^+ / (k^+ + k^-)$ and

$$\binom{N}{n} = \frac{N!}{n!(N-n)!}.$$

Although this may not be obvious at first, in Exercise 4 the mathematically inclined reader can use the method of substitution to confirm that the binomial distribution satisfies a time-independent version of (11.15).

Figure 11.4 shows several binomial probability distributions with parameters N and p varied. Given an ensemble of N two-state channels, these distributions represent the equilibrium probability of finding n channels in the open state. In the top row, the equilibrium open probability of $p = 0.5$ results in a centered distribution: The likelihood of observing n open channels is equal to the likelihood of observing $N - n$

open channels. In the bottom row $p = 0.75$, and the enhanced likelihood that channels are open is evident in the rightward shift of the distributions.

11.2.2 The Average Number of Open Channels

The equilibrium solution to the master equation for the two-state channel given by (11.16) is the binomial distribution, and thus the average number of open channels at equilibrium is $\langle N_O \rangle_\infty = Np$. But what about the time-dependence of the average number of open channels? Because the average number of open channels is given by

$$\langle N_O \rangle = \sum_{n=0}^N n P_O(n, t), \quad (11.17)$$

we can find an equation for $d\langle N_O \rangle/dt$ by multiplying (11.15) by n and summing. This gives

$$\begin{aligned} \frac{d\langle N_O \rangle}{dt} = & k^+ \sum_{n=0}^N n(N-n+1)P_O(n-1, t) - k^+ \sum_{n=0}^N n(N-n)P_O(n, t) \\ & + k^- \sum_{n=0}^N n(n+1)P_O(n+1, t) - k^- \sum_{n=0}^N n^2 P_O(n, t). \end{aligned} \quad (11.18)$$

In Exercise 6 the reader can show that this equation can be reduced to

$$\frac{d\langle N_O \rangle}{dt} = k^+ (N - \langle N_O \rangle) - k^- \langle N_O \rangle, \quad (11.19)$$

where

$$N - \langle N_O \rangle = \langle N_C \rangle. \quad (11.20)$$

Note that (11.19) is identical to the rate equation for a population of two-state channels derived by other means in Chapter 1. For the duration of this chapter we will refer to such an equation as an *average rate equation*. Also note that the equilibrium average number of open ($\langle N_O \rangle_\infty$) and closed ($\langle N_C \rangle_\infty$) channels can be found by setting the left-hand side of (11.19) to zero, that is,

$$\langle N_O \rangle_\infty = N \frac{k^+}{k^+ + k^-} = Np, \quad (11.21)$$

$$\langle N_C \rangle_\infty = N \frac{k^-}{k^+ + k^-} = N(1-p), \quad (11.22)$$

in agreement with our knowledge of the mean of a binomial distribution.

If we divide (11.19) by the total number of channels N , we find the average rate equation for the fraction of open channels

$$\frac{d\langle f_O \rangle}{dt} = k^+ (1 - \langle f_O \rangle) - k^- \langle f_O \rangle, \quad (11.23)$$

where $\langle f_O \rangle = \langle N_O \rangle / N$, $\langle f_C \rangle = \langle N_C \rangle / N$, and (11.20) implies $\langle f_O \rangle + \langle f_C \rangle = 1$. The equilibrium fractions of open and closed channels are $\langle f_O \rangle_\infty = k^+ / (k^+ + k^-) = p$ and $\langle f_C \rangle_\infty = k^- / (k^+ + k^-) = 1 - p$. We thus see explicitly for a two-state channel that the master equation implies an average rate equation of the sort introduced in Chapter 2. This is true in general.

11.2.3 The Variance of the Number of Open Channels

One advantage of beginning with a master equation is that in addition to the average rate equation, an evolution equation for the variance in the number of open channels can be derived. The variance in the number of open channels is defined as

$$\sigma_{N_O}^2 = \langle (N_O - \langle N_O \rangle)^2 \rangle = \sum_{n=0}^N (n - \langle N_O \rangle)^2 P_O(n, t). \quad (11.24)$$

Similarly, the variance in the number of closed channels is

$$\sigma_{N_C}^2 = \langle (N_C - \langle N_C \rangle)^2 \rangle = \sum_{n=0}^N (n - \langle N_C \rangle)^2 P_C(n, t). \quad (11.25)$$

Again, we are ultimately interested in the statistics of current fluctuations, so we focus on $\sigma_{N_O}^2$. For the two-state channel under consideration, it is shown in Exercise 8 that these quantities are equal.

Beginning with (11.24) and the master equation (11.15), it can be shown that the variance $\sigma_{N_O}^2$ satisfies the ODE

$$\frac{d\sigma_{N_O}^2}{dt} = -2(k^+ + k^-)\sigma_{N_O}^2 + k^+(N - \langle N_O \rangle) + k^-\langle N_O \rangle. \quad (11.26)$$

The equilibrium variance $(\sigma_{N_O}^2)_\infty$ is thus given by steady states of this equation. Setting the left-hand side of this expression to zero, we obtain

$$(\sigma_{N_O}^2)_\infty = N \frac{k^+ k^-}{(k^+ + k^-)^2} = Np(1 - p). \quad (11.27)$$

From this equation it is clear that the equilibrium variance is proportional to N , the total number of channels. However, a relative measure of the variance known as the *coefficient of variation* is more meaningful. The coefficient of variation of the number of open channels, CV_{N_O} , is given by the ratio of the standard deviation σ_{N_O} (the square root of the variance) to the mean $\langle N_O \rangle$. At equilibrium, we have

$$(CV_{N_O})_\infty = \frac{(\sigma_{N_O})_\infty}{\langle N_O \rangle_\infty} = \frac{1}{\sqrt{N}} \sqrt{\frac{k^-}{k^+}} = \sqrt{\frac{1-p}{Np}},$$

where the last equality is in agreement with the mean and variance of a binomially distributed random variable being Np and $Np(1-p)$, respectively. From this expression it is clear that the equilibrium coefficient of variation for the number of open channels

is inversely proportional to the square root of the number of channels N . Thus, in order to decrease this relative measure of channel noise by a factor of two, the number of channels must be increased by a factor of 4.

11.3 Fluctuations in Macroscopic Currents

When the voltage clamp technique is applied to isolated membrane patches, openings and closings of single ion channels can be observed. Recall the single-channel recordings of T-type Ca^{2+} currents shown in the top panel of Figure 11.2. Importantly, the bottom panel of Figure 11.2 shows that when several hundred single-channel recordings are summed, the kinetics of rapid activation and slower inactivation of the T-type Ca^{2+} current are evident. In this summed trace, the relative size of the fluctuations in the macroscopic current is much smaller than those observed in the single-channel recordings; however, the fluctuations in ionic current are still noticeable.

During voltage clamp recordings of large numbers of ion channels, stochastic gating leads to current fluctuations. For example, Figure 11.5B shows the time evo-

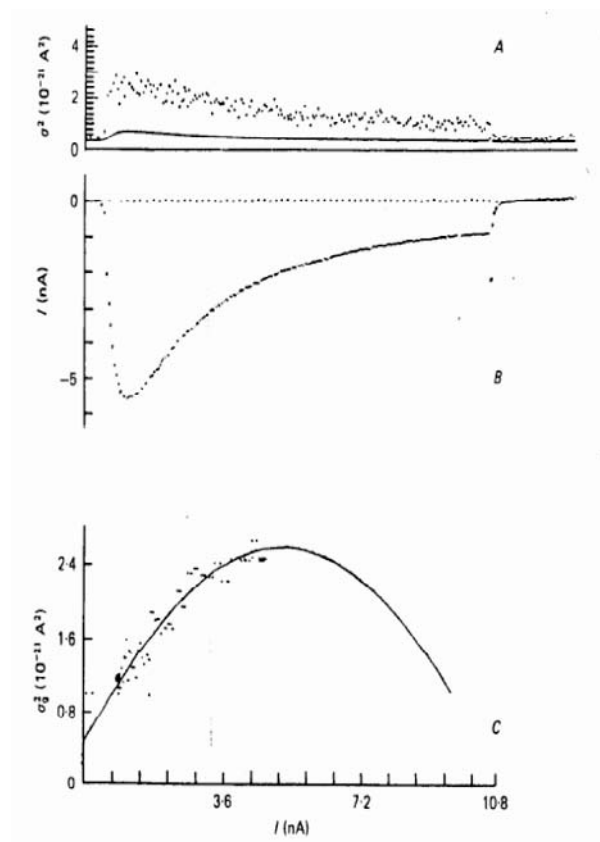


Figure 11.5 Variance and mean sodium current measured from voltage-clamped single myelinated nerve fibers from *Rana pipiens* depolarized to -15 mV after 50 ms prepulses to -105 mV. (A) Variance arising from the stochastic gating of sodium channels (dots) and thermal noise (solid line). (B) Mean current. (C) After carefully accounting for contributions to the variance due to thermal noise, the parabolic relationship between variance and mean current suggests $N=20,400$ sodium channels at this node of Ranvier each with single channel conductance of $i_{\text{unit}} = 0.55$ pA. Reprinted from Sigworth (1980).

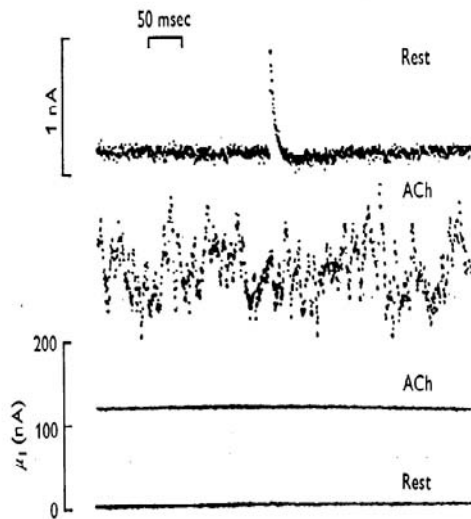


Figure 11.6 Acetylcholine-produced current noise due to fluctuations in ionic conductance of voltage-clamped end-plates of *Rana pipiens* nerve-muscle preparation. Iontophoretic application of ACh resulted in an increase in mean current as well as variance. The second trace, labeled "Rest," also shows a spontaneous miniature end-plate current. Reprinted from Anderson and Stevens (1973).

lution of the mean sodium current measured from voltage-clamped single myelinated nerve fibers of *Rana pipiens* (frog) that were depolarized to -15 mV after 50 ms pre-pulses to -105 mV. After a careful accounting for contributions to the variance of the sodium current due to thermal noise (Figure 11.5A, solid line), the variance arising from the stochastic gating of sodium channels remains (Figure 11.5A, dots). Figure 11.6 shows macroscopic current fluctuations induced by the iontophoretic application of acetylcholine (ACh) to voltage-clamped end-plates of a *Rana pipiens* nerve-muscle preparation. Interestingly, iontophoretic application of ACh increased the variance of the end-plate current as well as the mean. While the first trace in Figure 11.6 shows a spontaneous miniature end-plate current (sharp peak), the phenomenon of interest is the 10-fold increase in variance observed throughout the duration of the second trace (as compared to the first).

In order to understand the relationship between fluctuations in macroscopic currents and the underlying single-channel kinetics, consider the statistics of ionic current implied by the two-state channel model presented in the previous section. In the simplest case, the unitary current of each two-state channel will be a random variable taking the value zero when the channel is closed or a fixed value i_{unit} when the channel is open. That is, the unitary current will be a random variable I_{unit} given by

$$I_{\text{unit}} = \begin{cases} i_{\text{unit}} = g_{\text{unit}}(V - V_{\text{rev}}) & \text{when open,} \\ 0 & \text{when closed,} \end{cases} \quad (11.28)$$

where V is a fixed command voltage, V_{rev} is the reversal potential for the single-channel conductance g_{unit} , and i_{unit} is directly proportional to the conductance of the open channel. With these assumptions, it is straightforward to apply the results of Section

11.2 and derive the statistics of a fluctuating current that will result from N two-state channels with unitary current given by (11.28). The fluctuating macroscopic current will be a random variable defined by

$$I_{\text{macro}} = N_O i_{\text{unit}} \quad (0 \leq N_O \leq N),$$

where N_O is the number of open channels (also a random variable). Because the macroscopic current is directly proportional to N_O , we can use (11.17) to find the equilibrium average macroscopic current

$$\langle I_{\text{macro}} \rangle_{\infty} = i_{\text{unit}} \langle N_O \rangle_{\infty}.$$

Similarly, the equilibrium variance in the number of open channels, $(\sigma_{N_O}^2)_{\infty}$, given by (11.27), determines the equilibrium variance of the macroscopic current

$$(\sigma_{I_{\text{macro}}}^2)_{\infty} = i_{\text{unit}}^2 (\sigma_{N_O}^2)_{\infty}.$$

Recall that if we write $p = k^+ / (k^+ + k^-)$, the equilibrium mean and variance for the number of open channels are given by $\langle N_O \rangle_{\infty} = Np$ and $(\sigma_{N_O}^2)_{\infty} = Np(1-p)$. Thus, the equilibrium mean and variance for the macroscopic current are given by $\langle I_{\text{macro}} \rangle_{\infty} = i_{\text{unit}} Np$ and $(\sigma_{I_{\text{macro}}}^2)_{\infty} = i_{\text{unit}}^2 Np(1-p)$. Combining these expressions and eliminating p gives

$$(\sigma_{I_{\text{macro}}}^2)_{\infty} = i_{\text{unit}} \langle I_{\text{macro}} \rangle_{\infty} - \langle I_{\text{macro}} \rangle_{\infty}^2 / N, \quad (11.29)$$

where both $\langle I_{\text{macro}} \rangle_{\infty}$ and $(\sigma_{I_{\text{macro}}}^2)_{\infty}$ are parameterized by p .

Equation (11.29) is the basis of a standard technique of membrane noise analysis whereby current fluctuations can be used to estimate the number of ion channels in a membrane patch. By repeatedly manipulating the fraction of open channels p an estimate of $(\sigma_{I_{\text{macro}}}^2)_{\infty}$ as a function of $\langle I_{\text{macro}} \rangle_{\infty}$ is obtained. According to (11.29), the relationship will be parabolic with zero variance at $\langle I_{\text{macro}} \rangle_{\infty} = 0$ and $\langle I_{\text{macro}} \rangle_{\infty} = i_{\text{unit}} N$ and a maximum variance of $(\sigma_{I_{\text{macro}}}^2)_{\infty} = Ni_{\text{unit}}^2 / 4$ at $\langle I_{\text{macro}} \rangle_{\infty} = i_{\text{unit}} N / 2$. In Figure 11.5C this technique was applied to voltage-clamped single myelinated nerve fibers from *Rana pipiens*. Equation (11.29) and a visual fit resulting in a maximum of $(\sigma_{I_{\text{macro}}}^2)_{\infty} = 2.5 \times 10^{-21} \text{ A}^2$ at $\langle I_{\text{macro}} \rangle_{\infty} = 5 \text{ nA}$ suggests that $N = \langle I_{\text{macro}} \rangle_{\infty}^2 / (\sigma_{I_{\text{macro}}}^2)_{\infty} = 10,000$ and $i_{\text{unit}} = 1 \text{ pA}$. However, after carefully accounting for contributions to the variance due to thermal noise, an adjusted fit (solid line in Figure 11.5C) gives $N = 20,400$ sodium channels at this node of Ranvier and a unitary current of $i_{\text{unit}} = 0.55 \text{ pA}$ (see Sigworth 1980).

In Figure 11.7 this technique was applied to end-plate conductance fluctuations of *Rana pipiens* nerve-muscle preparation. Here, the equilibrium variance of the macroscopic conductance $(\sigma_{g_{\text{macro}}}^2)_{\infty}$ is plotted against the mean conductance $\langle g_{\text{macro}} \rangle_{\infty}$, where the macroscopic conductance is related to the unitary conductance through $g_{\text{macro}} = Ng_{\text{unit}}$. Using (11.29) and the relations

$$\langle g_{\text{macro}} \rangle_{\infty} = \frac{\langle I_{\text{macro}} \rangle_{\infty}}{V - V_{\text{rev}}}, \quad (\sigma_{g_{\text{macro}}}^2)_{\infty} = \frac{(\sigma_{I_{\text{macro}}}^2)_{\infty}}{(V - V_{\text{rev}})^2} \quad \text{and} \quad i_{\text{unit}} = g_{\text{unit}} (V - V_{\text{rev}}),$$

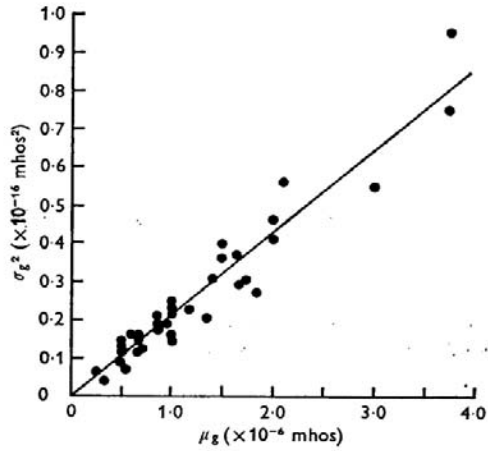


Figure 11.7 Variance of conductance fluctuations as a function of mean end-plate conductance of *Rana pipiens* nerve-muscle preparation. Because the unitary conductance of end-plate channels is small, the relationship is linear and the slope of $0.19 \times 10^{-10} \text{ mho} = 19 \text{ pS}$ gives the single-channel conductance. Reprinted from Anderson and Stevens (1973).

the reader can confirm that this relationship is also expected to be parabolic, that is,

$$\left(\sigma_{g_{\text{macro}}}^2\right)_{\infty} = g_{\text{unit}} \langle g_{\text{macro}} \rangle_{\infty} - \langle g_{\text{macro}} \rangle_{\infty}^2 / N.$$

However, because the unitary end-plate channel conductance of *Rana pipiens* nerve-muscle preparation is very small (quadratic term negligible), the relationship is nearly linear:

$$\left(\sigma_{g_{\text{macro}}}^2\right)_{\infty} = g_{\text{unit}} \langle g_{\text{macro}} \rangle_{\infty}.$$

Indeed, the slope of the line in Figure 11.7 gives a single channel conductance of 19 pS for the open end-plate channel.

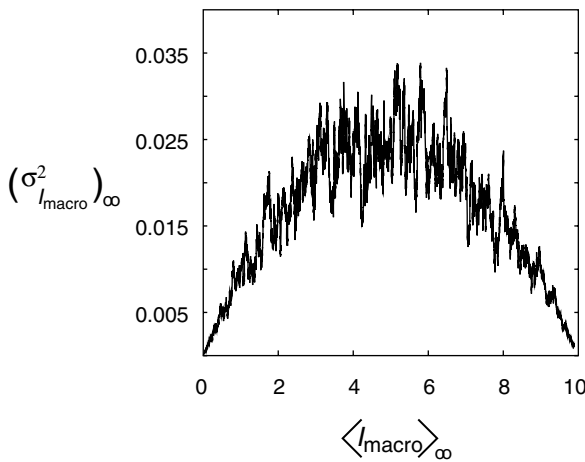


Figure 11.8 The parabolic relationship between the variance and mean of ionic current through $N = 10,000$ two-state channels each with single-channel conductance of $i_{\text{unit}} = 0.01 \text{ pA}$. The parabolic relationship between the variance $\left(\sigma_{I_{\text{macro}}}^2\right)_{\infty}$ and mean $\langle I_{\text{macro}} \rangle_{\infty}$ of current fluctuations is calculated from 100 simultaneously integrated Langevin equations.

11.4 Modeling Fluctuations in Macroscopic Currents with Stochastic ODEs

Figure 11.8 shows a simulation reproducing the parabolic relationship between the variance $(\sigma_{I_{\text{macro}}}^2)_{\infty}$ and mean, $\langle I_{\text{macro}} \rangle_{\infty}$, of current fluctuations due to the stochastic gating of ion channels. This simulation includes $N = 10,000$ identical two-state channels with unitary conductance of $i_{\text{unit}} = 0.01$ pA. A hundred trials were simultaneously performed and averaged to calculate the mean and variance as the open probability p ranged from 0 to 1. Because the methods discussed in Section 11.1.4 would require the declaration of a Markov variable with 10,001 possible states, the reader may be wondering how this simulation was performed.

Indeed, in simulating the stochastic gating of large numbers of ion channels, Monte Carlo methods becomes impractical. However, when N is large, fluctuations in macroscopic currents can instead be described using a stochastic ordinary differential equation, called a Langevin equation, that takes the form

$$\frac{df}{dt} = g(f) + \xi. \quad (11.30)$$

In this equation, the familiar deterministic dynamics given by $g(f)$ are supplemented with a rapidly varying random forcing term $\xi(t)$. Because ξ is a random function of time, solving (11.30) often means finding a solution $f(t)$ that satisfies the equation for a particular instantiation of ξ . Alternatively, if the statistics of ξ are given, we may be interested in deriving the statistics of the new random variable $f(t)$ that is formally defined by (11.30).

The most common fluctuating force to consider are the increments of a Wiener process. Similar to the unbiased random walk discussed in Chapter 12, a Wiener process $B(t)$ is a “Gaussian” random process that has zero mean

$$\langle B \rangle = 0 \quad (11.31)$$

and variance directly proportional to time,

$$\sigma_B^2 = \langle (B - \langle B \rangle)^2 \rangle = \langle B^2 \rangle = t. \quad (11.32)$$

Indeed, the instantiations of a Wiener process B_1 and B_2 shown in Figure 11.9 are similar to the random walks presented in Figure 12.4. Just as the increments of an unbiased random walk are $\pm\Delta x$ with equal probability, resulting in an increment with mean zero $\langle \Delta X \rangle = 0$, the increments of the numerical approximation to a Wiener process shown in Figure 11.9 are normally distributed with mean zero,

$$\langle \Delta B \rangle = 0.$$

In order to understand the variance of the increments of this simulated Wiener process, we must remember that unlike an unbiased random walk, a Wiener process is a continuous function of time, $B(t)$. A relevant statistic for the increments of a Wiener process is the two-time covariance or *autocorrelation function* $\langle \Delta B(t)\Delta B(t') \rangle$. Because

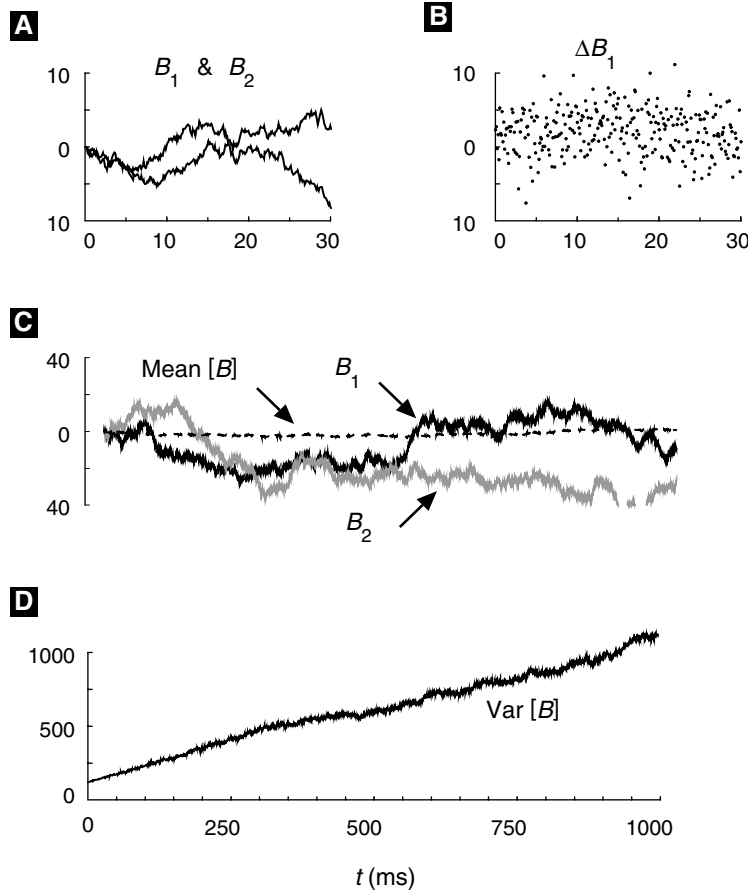


Figure 11.9 Two instantiations of a Wiener process, B_1 and B_2 , have trajectories similar to the random walks shown in Figure 12.4. The mean of 100 trials is near zero, while the variance of 100 trials increases linearly with time. In these simulations the increments (ΔB) are normally distributed with mean zero and variance $1/\Delta t$, where Δt is the integration time step.

nonoverlapping increments of a Wiener process are statistically independent and uncorrelated, $\langle \Delta B(t) \Delta B(t') \rangle = 0$ for $t' > t + \Delta t$ in Figure 11.9. In the limit as $\Delta t \rightarrow 0$ (i.e., for a “real” Wiener process), we might even write $dB(t)/dt = \xi(t)$, where $\langle \xi(t) \rangle = 0$ and

$$\langle \xi(t) \xi(t') \rangle = \delta(t - t'), \quad (11.33)$$

although technically this derivative does not exist. Equation (11.33) may appear unusual, especially if the reader is unfamiliar with the Dirac delta function, defined by $\delta(t) = 0$ for $t \neq 0$ and

$$\int_{-\infty}^{\infty} \delta(t) dt = 1.$$

A Wiener process $B(t)$ can be simulated by numerically integrating a piecewise constant approximation to the Wiener increment $\Delta B(t)$. The Wiener increment (Figure 11.9B) is a normally distributed random variable with zero mean that is held fixed during the time interval $[t, t + \Delta t]$ and updated after the integration time step is complete. Integrating this erratic function of time results in the Wiener trajectories of Figure 11.9A and Figure 11.9C. If we rewrite (11.33) to account for this piecewise constant approximation to the Wiener increments, we obtain

$$\langle \Delta B(t) \Delta B(t') \rangle = \begin{cases} 1/\Delta t, & t' \in [t, t + \Delta t], \\ 0 & \text{otherwise.} \end{cases}$$

Like the unbiased random walk, the variance of this simulated Wiener process is proportional to time as shown in Figure 11.9D. The reader can confirm through simulations that in order to achieve this macroscopic behavior, the variance of the Wiener increments $\Delta B(t)$ must be adjusted according to the integration time step (i.e., $\text{Var}[\Delta B] = 1/\Delta t$ gives $\text{Var}[B] = t$).

11.4.1 Langevin Equation for an Ensemble of Two-State Channels

In order to use a Langevin equation of the form of (11.30) to simulate a large number of ion channels, we must make an appropriate choice for both the deterministic function $g(f)$ as well as the statistics of the random variable ξ . Recalling the average rate equation for the dynamics of the open fraction of channels (11.23), we write

$$\frac{df_O}{dt} = k^+ (1 - f_O) - k^- f_O + \xi \quad (11.34)$$

$$= -\frac{f_O - \langle f_O \rangle_\infty}{\tau_f} + \xi, \quad (11.35)$$

where $f_O = N_O/N$ is a random variable, the fluctuating fraction of open channels, $\langle f_O \rangle_\infty = k^+ / (k^+ + k^-)$, and $\tau_f = 1 / (k^+ + k^-)$. For (11.35) to be meaningful, we must specify the statistics of ξ . An appropriate choice for ξ is a fluctuating function of time that has zero mean,

$$\langle \xi(t) \rangle = 0,$$

and an autocorrelation function given by

$$\langle \xi(t) \xi(t') \rangle = \gamma \delta(t - t').$$

By methods of statistical physics beyond the scope of this book, γ can be shown to be inversely proportional to N and proportional to the sum of the rates of both the $O \rightarrow C$ and $C \rightarrow O$ transitions, that is,

$$\gamma(f_O) = \frac{k^+ (1 - f_O) + k^- f_O}{N}. \quad (11.36)$$

An appropriate choice for ξ is thus $\xi = \sqrt{\gamma} \Delta B$, where the ΔB are the increments of a Wiener process.

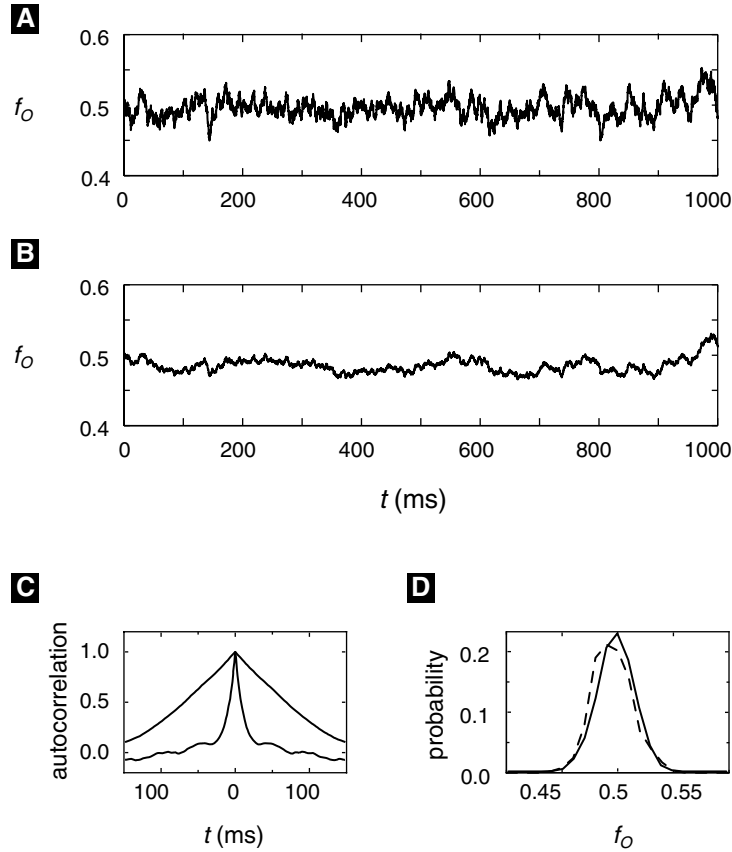


Figure 11.10 (A,B) The open fraction f_O of 1000 two-state ion channels simulated using a Langevin equation. Transition rates are ten times faster in (A) than (B) so that the time constant τ_f is 10 and 100 ms, respectively. (C) Numerically calculated autocorrelation function of f_O . (D) The equilibrium mean and variance of f_O are approximately equal in the two cases.

Although we haven't fully justified this choice for ξ , we can check that this random variable and (11.35) define the random variable f_O in a manner consistent with the work in previous sections. To do this we use the fluctuation–dissipation theorem (Keizer 1987; Gardiner 1997) from statistical physics that relates γ , which occurs in the correlation function of ξ , to the equilibrium variance of f_O . The relationship depends on the relaxation time constant τ_f and is given by

$$\gamma_\infty = \frac{2 \left(\sigma_{f_O}^2 \right)_\infty}{\tau_f}. \quad (11.37)$$

Using (11.27), and remembering that $\left(\sigma_{f_O}^2 \right)_\infty = \left(\sigma_{N_O}^2 \right)_\infty / N^2$, the reader can confirm that the last equality holds at equilibrium.

Stochastic simulations of the open fraction, f_O , of 1000 two-state ion channels calculated by integrating (11.35) are shown in Figure 11.10. The transition rates used were $k^+ = k^- = 0.05/\text{ms}$ in panel (A) and $k^+ = k^- = 0.005/\text{ms}$ in panel (B), giving time constants (τ_f) of 10 and 100 ms and equilibrium open fraction $\langle f_O \rangle_\infty = p = 0.5$ in both cases. This difference in relaxation time constants is evident in the (normalized) autocorrelation functions compared in C. It can be shown that for an infinitely long simulation the autocorrelation functions for f_O is

$$\langle f_O(t)f_O(t') \rangle = \left(\sigma_{f_O}^2 \right)_\infty e^{-|t-t'|/\tau_f}.$$

The narrower autocorrelation function in Figure 11.10C thus corresponds to the case with small time constant τ_f . Note that although the time constant for relaxation to $\langle f_O \rangle_\infty = 0.5$ is faster in A than in B, the equilibrium variance $\left(\sigma_{f_O}^2 \right)_\infty$ shown in Figure 11.10D is approximately equal in the two cases, as expected according to (11.27).

11.4.2 Fokker–Planck Equation for an Ensemble of Two-State Channels

Rather than calculating trajectories for the fraction of open channels f_O using a Langevin equation, an alternative is to calculate the evolution of the probability distribution function (PDF) for f_O . While the binomial distribution encountered in Section 11.2 is an example of a discrete probability distribution (N_O takes on $N + 1$ discrete values), the Langevin equation for f_O (11.35) implies that f_O can take on any value on the interval $[0,1]$. Thus, the PDF for f_O is continuous and defined as

$$P(f, t) df = \text{Prob}\{f(t) < f_O < f(t) + df\},$$

where conservation of probability gives

$$\int_0^1 P(f, t) df = 1. \quad (11.38)$$

We can write an evolution equation for $P(f, t)$, known as a Fokker–Planck equation, that corresponds to the Langevin description given by (11.35):

$$\frac{\partial P(f, t)}{\partial t} = -\frac{\partial}{\partial f} [J_{\text{adv}}(f, t) + J_{\text{dif}}(f, t)]. \quad (11.39)$$

In this equation, $J_{\text{adv}}(f, t)$ is a probability flux due to advection (that is, transport) governed by the deterministic terms in (11.35):

$$J_{\text{adv}}(f, t) = -\frac{f - \langle f_O \rangle_\infty}{\tau_f} P(f, t). \quad (11.40)$$

In contrast, $J_{\text{dif}}(f, t)$ is a diffusive flux that accounts for the spread of probability induced by the random variable ξ . This diffusive probability flux is given by

$$J_{\text{dif}}(f, t) = -\frac{1}{2} \frac{\partial}{\partial f} [\gamma(f) P(f, t)], \quad (11.41)$$

where γ is given by (11.36). Rewriting (11.40) in terms of the total probability flux $J_{\text{tot}} = J_{\text{adv}} + J_{\text{dif}}$, we have

$$\frac{\partial P(f, t)}{\partial t} = -\frac{\partial J_{\text{tot}}(f, t)}{\partial f}, \quad (11.42)$$

with associated boundary conditions

$$J_{\text{tot}}(0, t) = J_{\text{tot}}(1, t) = 0$$

that imply no flux of probability out of the physiological range for f_O . An appropriate choice of initial conditions would be $P(f, 0) = \delta(f - \langle f_O \rangle_\infty)$, implying that the system is known to be in equilibrium at $t = 0$.

Setting the left-hand side of (11.39) equal to zero, we see that the equilibrium probability distribution $P_\infty(f)$ solves $J_{\text{tot}}^\infty = 0$. That is,

$$-\frac{f - \langle f_O \rangle_\infty}{\tau_f} P_\infty(f) - \frac{1}{2} \frac{d}{df} [\gamma(f) P_\infty(f)] = 0. \quad (11.43)$$

This differential equation can be solved numerically. However, we obtain more insight by approximating $\gamma(f)$ by

$$\gamma_\infty = \frac{k^+ (1 - \langle f_O \rangle_\infty) + k^- \langle f_O \rangle_\infty}{N}.$$

This procedure is valid when fluctuations of f_O away from equilibrium, $\langle f_O \rangle_\infty$, are small (that is, when N is large). If we make this approximation, it can be shown that the probability distribution

$$P_\infty(f) = A \exp \left[\frac{f (2 \langle f_O \rangle_\infty - f)}{\gamma_\infty \tau_f} \right] \quad (11.44)$$

satisfies (11.43), where the normalization constant A is chosen to satisfy conservation of probability (11.38). While this expression may not look familiar, when γ_∞ is sufficiently small (N is sufficiently large), $P_\infty(f)$ is well approximated by the Gaussian

$$P_\infty(f) = \frac{1}{\sqrt{2\pi} (\sigma_{f_O}^2)_\infty} \exp \left[-\frac{(f - \langle f_O \rangle_\infty)^2}{2 (\sigma_{f_O}^2)_\infty} \right].$$

At equilibrium f_O will be a normally distributed random variable with mean $\langle f_O \rangle_\infty$ and variance $(\sigma_{f_O}^2)_\infty = \gamma_\infty \tau_f / 2$, in agreement with (11.37). The distribution $P_\infty(f)$ is approximately Gaussian for $N = 1000$ as shown in Figure 11.10D.

11.5 Membrane Voltage Fluctuations

In Section 11.3 we discussed macroscopic current fluctuations experimentally observed in voltage clamp recordings and a membrane noise analysis. In this section we will

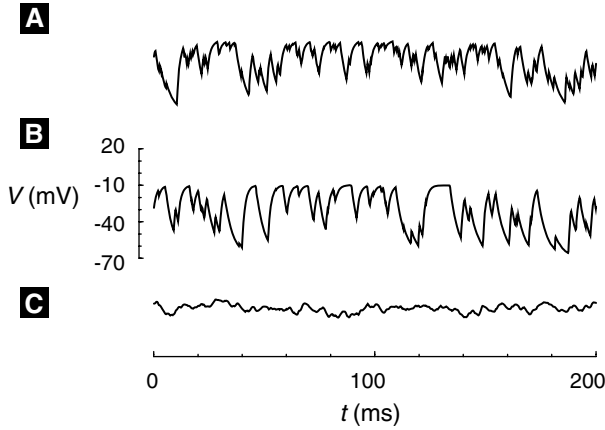


Figure 11.11 Membrane voltage fluctuations due to the stochastic gating of one or more sodium channels. (A,B) Single channel simulations. Transition probabilities are a factor of two slower in (B), leading to longer dwell times and fewer transitions as evidenced by 'kinks' in graph. (C) Twenty channels are simulated. As the number of sodium channels increases, the variance in membrane voltage decrease.

simulate electrical recordings in which the membrane potential is not clamped, but rather fluctuates under the influence of two-state ion channels. Although a misnomer, such measurements are referred to as *current clamp* recordings. For now we assume that ion channel gating is voltage-independent.

Simulations of membrane voltage fluctuations due to the stochastic gating of a single sodium channel obeying the transition-state diagram (11.1) are shown in Figure 11.11A and Figure 11.11B. The gating of the two-state channel is simulated using Monte Carlo methods, while membrane voltage is simultaneously calculated using the current balance equation

$$C \frac{dV}{dt} = -g_L (V - V_L) - g_{Na} (V - V_{Na}), \quad (11.45)$$

where g_L is leakage conductance with reversal potential $V_L = -70$ mV, and g_{Na} (a random variable taking values of 0 or g_{Na}^{\max} depending on channel state) is a sodium conductance with reversal potential $V_{Na} = 60$ mV. Because transition probabilities are a factor of two slower in Figure 11.11B, longer dwell times and fewer transitions are observed. For comparison, Figure 11.11C shows the result when twenty channels are simulated. Here g_{Na} takes on 21 possible values between 0 and g_{Na}^{\max} and as a consequence the variance in the fluctuating membrane voltage decreases.

Membrane voltage fluctuations such as those shown in Figure 11.11 can also be modeled by tracking the evolution of probability distribution functions (PDFs) for membrane voltage conditioned on the state of the ion channel. The governing equations are coupled partial differential equations each of which is similar to the advective component of the Fokker-Planck equations described above. We will refer to this method as the *ensemble density approach*.

If membrane voltage fluctuations are due to a single two-state sodium channel, there are two relevant conditional PDFs,

$$P_C(v, t) dv = \text{Prob}\{v < V < v + dv | C, t\},$$

$$P_O(v, t) dv = \text{Prob}\{v < V < v + dv | O, t\},$$

where $P_C(v, t)$ and $P_O(v, t)$ are conditioned on the channel being closed or open, respectively. Conservation of probability implies

$$\int_{-\infty}^{\infty} P_C(v, t) dv = 1, \quad \int_{-\infty}^{\infty} P_O(v, t) dv = 1.$$

The equations for the evolution of these conditional PDFs are

$$\frac{\partial}{\partial t} P_C(v, t) = -\frac{\partial}{\partial v} J_C(v, t) - k^+ P_C(v, t) + k^- P_O(v, t), \quad (11.46)$$

$$\frac{\partial}{\partial t} P_O(v, t) = -\frac{\partial}{\partial v} J_O(v, t) + k^+ P_C(v, t) - k^- P_O(v, t), \quad (11.47)$$

where $J_C(v, t)$ and $J_O(v, t)$ are advective probability fluxes due to membrane voltage obeying the current balance equation (11.45):

$$J_C(v, t) = -\frac{1}{C} [g_L (v - V_L)] P_C(v, t),$$

$$J_O(v, t) = -\frac{1}{C} [g_L (v - V_L) + g_{\text{Na}}^{\text{max}} (v - V_{\text{Na}})] P_O(v, t).$$

Notice that the sodium current term occurs only in $J_O(v, t)$, because if the channel is closed, $g_{\text{Na}} = 0$. The reaction terms that appear in (11.46) and (11.47) account for probability flux due to the stochastic gating of the sodium channel. Regardless of membrane voltage, the conditional probability $P_C(v, t)$ can decrease due to channel opening at a rate of $k^+ P_C(v, t)$ and increase due to closing of open channels at a rate of $k^- P_O(v, t)$. The reaction terms occur with opposite sign because any increase or decrease in the conditional probability $P_C(v, t)$ due to a channel gating implies commensurate change in $P_O(v, t)$.

The equilibrium conditional probability distribution functions for the membrane voltage, $P_C^\infty(v)$ and $P_O^\infty(v)$, calculated numerically from (11.46) and (11.47), are shown in Figure 11.12A. The simulation ran for 1 second, corresponding to approximately 1000 changes in channel state. As expected, $P_O^\infty(v)$ is shifted toward the right (depolarized V) relative to $P_C^\infty(v)$. The astute reader will note that the PDFs are not symmetric, indicating that when the channel is open probability advects toward V_{Na} faster than it advects toward V_L when the channel is closed; i.e., an open sodium channel leads to a smaller membrane time constant. In Figure 11.12B, the rate constants k^+ and k^- are a factor of ten slower. In this case, more probability accumulates near both V_L and V_{Na} .

11.5.1 Membrane Voltage Fluctuations with an Ensemble of Two-State Channels

The ensemble density formulation described above can be extended to the case where membrane voltage fluctuations are due to an ensemble of N two-state channels. If we write $P_O(n, v, t)$ for the conditional probability density for membrane voltage given n

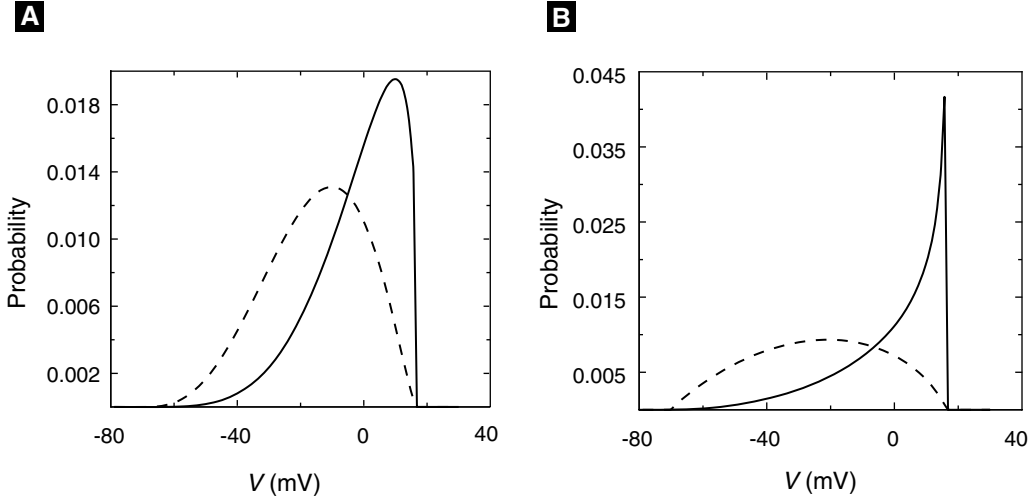


Figure 11.12 Equilibrium conditional probability distribution functions (PDFs), $P_C^\infty(v)$ (dotted lines) and $P_O^\infty(v)$ (solid lines) for the membrane voltage conditioned on the state of a single two-state sodium channel. In (A), $k^+ = k^- = 1/\text{ms}$, while for (B) the transition probabilities are a factor of two slower.

open sodium channels, we have

$$\begin{aligned} \frac{\partial}{\partial t} P_O(n, v, t) = & -\frac{\partial}{\partial v} J_O(n, v, t) \\ & + k^+(N - n + 1)P_O(n - 1, v, t) - k^+(N - n)P_O(n, v, t) \\ & + k^-(n + 1)P_O(n + 1, v, t) - k^-n P_O(n, v, t), \end{aligned} \quad (11.48)$$

where the reaction terms are based on the master equation formulation presented in Section 11.2.1, $J_O(n, v, t)$ is given by

$$J_O(n, v, t) = -\frac{1}{C} \left[g_L (v - V_L) + g_{\text{Na}}^{\text{max}} \frac{n}{N} (v - V_{\text{Na}}) \right] P_O(n, v, t),$$

and $g_{\text{Na}}^{\text{max}}$ is the sodium conductance when all N channels are open. Note that (11.48) represents $N + 1$ coupled partial differential equations, one for each $P_O(n, v, t)$, where $0 \leq n \leq N$.

Figure 11.13 shows equilibrium conditional PDFs $P_O^\infty(n, v)$ for membrane voltage fluctuations induced by 20 two-state sodium channels. These PDFs are calculated by numerically solving (11.48) until a steady state is achieved. Careful inspection of the figure shows that in the case of high n (more open channels) the equilibrium distribution of membrane voltage is shifted toward V_{Na} . Note that these PDFs appear to be consistent with a binomial distribution for the total equilibrium probability for a given

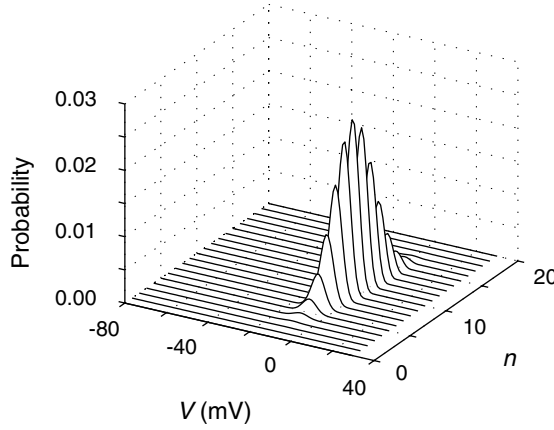


Figure 11.13 Conditional probability distribution functions for membrane voltage fluctuations due to stochastic gating of 20 two-state sodium channels. Parameters as in Figure 11.12A.

value of n . That is,

$$P_O^\infty(n) = \int_{-\infty}^{\infty} P_O^\infty(n, v) dv$$

is in agreement with (11.16).

11.6 Stochasticity and Discreteness in an Excitable Membrane Model

Using the results of previous sections, we are prepared to explore the consequences of stochasticity and discreteness in an excitable membrane model. The deterministic Morris–Lecar model is

$$C \frac{dV}{dt} = I_{\text{app}} - g_L(V - V_L) - g_K w(V - V_K) - g_{\text{Ca}} m_\infty(V - V_{\text{Ca}}) \quad (11.49)$$

$$\frac{dw}{dt} = \frac{w_\infty - w}{\tau}, \quad (11.50)$$

where the activation function for the Ca^{2+} current, $m_\infty(V)$; the activation function for the K^+ current, $w_\infty(V)$; and voltage-dependent time scale for activation of K^+ current, $\tau(V)$, are given in Chapter 2.

In (11.50), w is usually thought to represent the fraction of open K^+ channels. However, we now understand that this differential equation is actually an average rate equation similar to (11.23). To be clear, let us write this deterministic average rate equation as

$$\frac{d\langle w \rangle}{dt} = \frac{w_\infty - \langle w \rangle}{\tau},$$

where w (a random variable) represent the fraction of open K^+ channels. The reader can easily verify that this average rate equation corresponds to the two-state kinetic

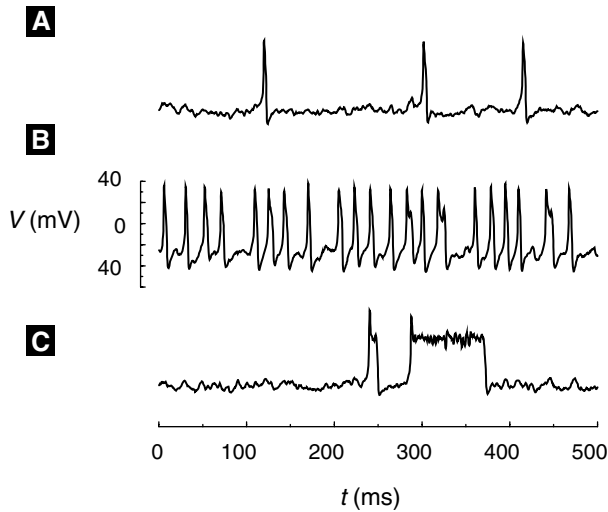


Figure 11.14 Morris–Lecar simulations including stochastic gating of 100 K^+ channels. (A) Spontaneous excitability driven by channel noise is observed when $I_{app} = 10$ and the deterministic model is excitable. (B) Stochastic oscillations are observed when $I_{app} = 12$ and the deterministic model is oscillatory. (C) Stochastic bistability is observed when the deterministic model is bistable ($I_{app} = 12$ and $v_3 = 15$ mV rather than standard value of 10 mV).

induced by this simulated channel noise (Figure 11.14A). We will refer to this phenomenon as “stochastic excitability,” because it is understood as a sampling of the excitable phase space of the deterministic model made possible by membrane potential fluctuations due to the stochastic gating of K^+ channels. The (V, w) phase plane trajectories for Figure 11.14 are shown in Figure 11.15. The discreteness and stochasticity of the K^+ gating variable w allows trajectories to fluctuate around the fixed point of the deterministic model seen in the lower left of Figure 11.15. Occasionally, K^+ channels spontaneously inactivate (w fluctuates toward 0) and a regenerative Ca^{2+} current leads to an action potential. This type of spontaneous activity has been observed in stochastic versions of the Hodgkin–Huxley equations (Chow and White 1996; Fox 1997) and is thought to influence subthreshold membrane potential oscillations and excitability of stellate neurons of the medial entorhinal cortex of the hippocampal region (White et al. 1995; White et al. 2000).

In Figure 11.14B parameters are such that the deterministic model (as $N \rightarrow \infty$) is oscillatory. However, when $N = 100$ channel noise results in irregular oscillations. In Figure 11.14B stochastic bistability is observed. When parameters are chosen so that the deterministic model is bistable, channel noise allows the alternate sampling of two stable fixed points in the (V, w) phase plane, a phenomenon known as basin hopping.

11.6.2 The Ensemble Density Approach Applied to the Stochastic Morris–Lecar Model

The ensemble density approach described in Section 11.4.2 can be applied to the stochastic Morris–Lecar model described above. The evolution equations for the

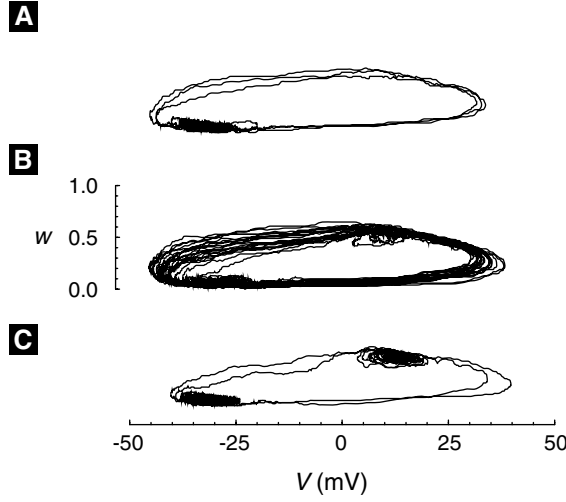


Figure 11.15 Morris–Lecar simulations with stochastic gating of 100 K^+ channels shown in the (V, w) phase plane. Panels correspond to (A) stochastic excitability, (B) oscillations, and (C) bistability shown in Figure 11.14.

conditional PDFs take the form

$$\begin{aligned} \frac{\partial}{\partial t} P_O(n, v, t) = & -\frac{\partial}{\partial v} J_O(n, v, t) \\ & + \alpha(v)(N - n + 1)P_O(n - 1, v, t) \\ & - \alpha(v)(N - n)P_O(n, v, t) \\ & + \beta(v)(n + 1)P_O(n + 1, v, t) - \beta(v)nP_O(n, v, t). \end{aligned} \quad (11.51)$$

This form is similar to (11.48) except that the transition probabilities are now voltage-dependent, and the probability fluxes $J_O(n, v, t)$ are given by the Morris–Lecar current balance equation (11.49). That is,

$$J_O(n, v, t) = -\frac{1}{C} \left[I_{\text{app}} - g_L(v - V_L) - g_K^{\text{max}} \frac{n}{N} (v - V_K) - g_{\text{Ca}} m_{\infty}(v - V_{\text{Ca}}) \right] P_O(n, v, t).$$

Figure 11.16 shows equilibrium PDFs for the membrane voltage of the stochastic Morris–Lecar model conditioned on the number of open K^+ channels. These equilibrium PDFs are steady-state solutions to (11.51) and correspond to the three types of trajectories shown in Figure 11.15. The amount of time that trajectories spend in different regions of the (V, w) phase plane is reflected in these distributions. It is clear from Figure 11.15A that the Morris–Lecar model exhibiting stochastic excitability spends a large proportion of time near the threshold for excitation.

11.6.3 Langevin Formulation for the Stochastic Morris–Lecar Model

To consider the behavior of the Morris–Lecar model under the influence of channel noise from a large number of K^+ channels, it is most convenient to use the Langevin formulation presented in Section 11.4.1. We do this by supplementing the rate equation for the average fraction of open K^+ channels, (11.50), with a rapidly varying forcing

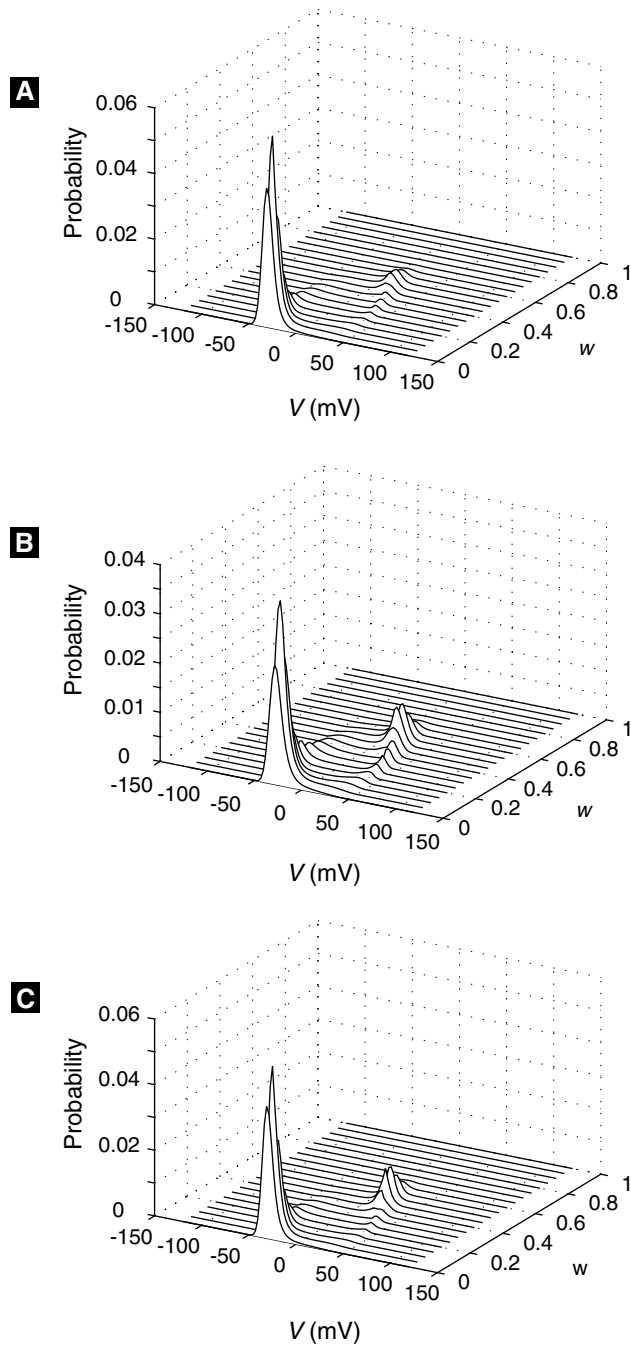


Figure 11.16 Probability distribution functions for the membrane voltage of the stochastic Morris-Lecar model conditioned on the number of open K^+ channels. The equilibrium PDFs show evidence of stochastic excitability (A), oscillations (B), and bistability (C), corresponding to the trajectories shown in Figure 11.15.

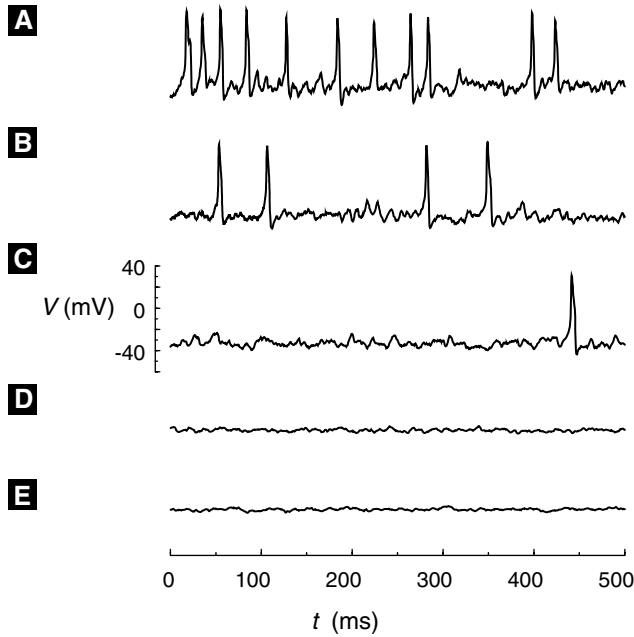


Figure 11.17 The stochastic Morris–Lecar model simulated using a Langevin equation for w , the fraction of open K^+ channels. As the number of K^+ channels is increased ($N = 25, 50, 100, 500$, or 1000) spontaneous action potentials induced by stochastic gating are eliminated. For large N , the model is excitable, but essentially deterministic; i.e., fluctuations in w are small and spontaneous action potentials are no longer observed without applied current.

term

$$\frac{dw}{dt} = \frac{w_\infty - w}{\tau} + \xi,$$

where w is a random variable, $\langle \xi \rangle = 0$, and the autocorrelation function of ξ is given by

$$\langle \xi(t)\xi(t') \rangle = \gamma(w, V)\delta(t - t').$$

Following (11.36), $\gamma(w, V)$ is chosen to be

$$\gamma(w, V) = \frac{\alpha(1-w) + \beta w}{N} = \frac{1}{N} \frac{(1 - 2w_\infty)w + w_\infty}{\tau}. \quad (11.52)$$

Thus, ξ is a random variable defined by $\xi = \sqrt{\gamma(w, V)}\Delta B$, where the ΔB are the increments of a Wiener process.

Figure 11.17 presents stochastic Morris–Lecar model simulations implemented using the Langevin formulation described above. Interestingly, the existence of stochastic excitability depends on the the number of K^+ channels included. When N is relatively small ($N = 25, 50, 100$) membrane potential fluctuations are large, and spontaneous action potentials are frequent. However, when more K^+ channels are included ($N = 500, 1000$), the model becomes essentially deterministic. Although the model is still excitable, as $N \rightarrow \infty$ fluctuations in w become smaller, and spontaneous action potentials are no longer observed.

Suggestions for Further Reading

- *Handbook of stochastic methods for physics, chemistry, and the natural sciences*, G.W. Gardiner. This is an accessible introduction to stochastic methods including Markov systems, stochastic differential equations, Fokker–Planck equations, and master equations (Gardiner 1997).
- *Spontaneous action potentials due to channel fluctuations*, C.C. Chow and J.A. White. A theoretical and numerical analysis of the Hodgkin–Huxley equations when stochastic ion channel dynamics are included (Chow and White 1996).
- *Stochastic versions of the Hodgkin–Huxley equations*, R.F. Fox. A presentation of master equation and Langevin descriptions of the Hodgkin–Huxley equations with stochastic ion channel dynamics (Fox 1997).
- *Channel noise in neurons*, J.A. White, J.T. Rubinstein, and A.R. Kay. A good review of stochastic gating of voltage-dependent ion channels and channel noise in neurons (White et al. 2000).

11.7 EXERCISES

1. Consider a single GLUT molecule and the four states (S_1, S_2, S_3, S_4) and transitions shown in Figure 3.1. Define s to be a random variable taking values $s \in \{1, 2, 3, 4\}$ corresponding to these four states and write $P_i(t)$ to represent the probability that $s(t) = i$, that is, the molecule is in state i at time t . Write an equation that indicates conservation of probability, that is, an equation resulting from the fact that the molecule must be in one of the four states.
2. Consider the possibility that the GLUT transporter (see previous exercise) is in state 1 at time t . What is the probability that in a short interval of time $[t, t + \Delta t]$ the GLUT transporter will associate with glucose, thereby transitioning out of state 1 and into state 2? What is the conditional probability, given that the channel is in state 1, of a $1 \rightarrow 2$ transition occurring during this interval?
3. Figure 3.1 and Table 3.1 indicate four possible ways for the GLUT transporter to enter or leave state 1. Accounting for all of these, we can write

$$P_1(t + \Delta t) = P_1(t) - k_{12}[G]_{\text{out}}P_1(t)\Delta t - k_{14}P_1(t)\Delta t + k_{21}P_2(t)\Delta t + k_{41}P_4(t)\Delta t.$$

Write three additional equations relating $P_i(t + \Delta t)$ and $P_i(t)$ for $i = \{2, 3, 4\}$ and take the limit $\Delta t \rightarrow 0$ to derive the a system of ODEs governing changes in probabilities for a single GLUT molecule being in states 1 through 4.

4. Use the method of substitution to confirm that the binomial distribution given by (11.16) is the steady state of the master equation for the two-state ion channel (11.15). Begin with a time-independent version of (11.15),

$$0 = k^+(N - n + 1)P_O^\infty(n - 1) - k^+(N - n)P_O^\infty(n) + k^-(n + 1)P_O^\infty(n + 1) - k^-nP_O^\infty(n);$$

and substitute $P_O^\infty(n-1)$, $P_O^\infty(n)$, and $P_O^\infty(n+1)$ according to (11.16). Remember that $p = k^+/(k^+ + k^-)$ and $1-p = k^-/(k^+ + k^-)$. After some algebra you will find that in order to balance the k^+ and k^- terms, one must have

$$(N-n+1) \binom{N}{n-1} = n \binom{N}{n},$$

$$(n+1) \binom{N}{n+1} = (N-n) \binom{N}{n},$$

as is indeed the case.

- Using (11.17) as a guide, write an expression for the average number $\langle N_C \rangle$ of closed channels in terms of $P_C(n, t)$. Then show that $N - \langle N_O \rangle = \langle N_C \rangle$, as stated in (11.20). Hint: You will need to use $P_C(n, t) = P_O(N-n, t)$ and $\sum_{n=0}^N n P_O(N-n, t) = \sum_{n=0}^N (N-n) P_O(n, t)$.
- Using the result of Exercise 5, confirm that (11.18) is equivalent to (11.19). In order to do so, you will need to show that

$$-\langle N_O \rangle = \sum_{n=0}^N n(n+1) P_O(n+1, t) - \sum_{n=0}^N n^2 P_O(n, t)$$

and

$$\langle N_C \rangle = \sum_{n=0}^N n(N-n+1) P_O(n-1, t) - \sum_{n=0}^N n(N-n) P_O(n, t).$$

- Equation (11.18) is the master equation for the two-state channel with kinetic scheme given by (11.1). Derive the the master equation for the GLUT transporter shown in Figure 3.1.
- Show that in the case of the two-state channel, the variances defined with respect to fluctuations in open channel number ($\sigma_{N_O}^2$) and closed channel number ($\sigma_{N_C}^2$), are equal. You will need some of the relations from Exercise 5 as well as (11.24) and (11.25).
- Confirm (11.26), the equation for the time-dependence of the variance of the two-state channel. Hint: Differentiate (11.24) to obtain

$$\frac{d\sigma_{N_O}^2}{dt} = \sum_{n=0}^N \left[-2(n - \langle N_O \rangle) \frac{d\langle N_O \rangle}{dt} P_O(n, t) + (n - \langle N_O \rangle)^2 \frac{dP_O(n, t)}{dt} \right]. \quad (11.53)$$

Now check to see whether the right-hand sides of (11.26) and (11.53) are equal. Use (11.19) and (11.15) as well as

$$\sum_{n=0}^N (n - \langle N_O \rangle)^2 (N-n+1) P_O(n-1, t) = \sum_{n=0}^{N-1} (n+1 - \langle N_O \rangle)^2 (N-n) P_O(n, t),$$

$$\sum_{n=0}^N (n - \langle N_O \rangle)^2 (n+1) P_O(n+1, t) = \sum_{n=1}^N (n-1 - \langle N_O \rangle)^2 n P_O(n, t).$$

- Simulate the four-state GLUT transporter shown in Figure 3.1 by implementing a Markov process with transition probability matrix

$$Q = \begin{bmatrix} D_1 & k_{21}\Delta t & 0 & k_{41}\Delta t \\ k_{12}[G]_{\text{out}}\Delta t & D_2 & k_{32}\Delta t & 0 \\ 0 & k_{23}\Delta t & D_3 & k_{43}\Delta t \\ k_{14}\Delta t & 0 & k_{34}[G]_{\text{in}}\Delta t & D_4 \end{bmatrix},$$

where the diagonal entries (D_1, D_2, D_3, D_4) are such that each column sums to 1.

11. Confirm the form of the time-invariant conditional PDFs shown in Figure 11.12.
 12. Reproduce simulations from Figure 11.14, Figure 11.15, and Figure 11.17.
-